The International Journal of Advanced Manufacturing Technology (2019) 103:3887–3899
https://doi.org/10.1007/s00170-019-03763-6

ORIGINAL ARTICLE

Effect of micro-textures on cutting fluid lubrication of cemented carbide tools

Dongliang Ge[1] · Jianxin Deng[1] · Ran Duan[1] · Yayun Liu[1] · Xuemu Li[1] · Hongzhi Yue[1]

Received: 11 January 2019 / Accepted: 15 April 2019 / Published online: 11 May 2019
© Springer-Verlag London Ltd., part of Springer Nature 2019

Abstract
Severe friction at the cutter-chip interface increases tool surface wear and reduces tool life. The friction could be reduced by introducing cutting fluids between cutter and chip. The lubrication of cutting fluids depends on its penetration. The ability of cutting fluids to penetrate into the cutting zone can be enhanced by the surface texture of the cutters. In this paper, microgroove-liked textures with different groove width were fabricated on the rake-face of the cemented carbide YS8 cutters with femtosecond laser. The effect of micro-textures on the lubrication of cutting fluids in cutting zone was investigated in cutting H13 hot die steel tests with textured and non-textured cutters under full lubrication. Results showed that micro-textures enhanced penetration of the cutting fluid, improved the lubrication in the cutter-chip interface, and significantly reduced cutting force and tool wear compared to untextured tools. The micro-textured tool with groove width of 50 μm had the best performance among all tested tools. Mechanism responsible was found that cutting fluids can continuously penetrate into the cutting contact area through the sufficient space provided by the microgrooves on the rake-face.

Keywords Surface texturing · Cutting fluids · Lubrication · Cutting tools

1 Introduction

There is severe friction and adhesion between the rake-face of tools and the bottom side of the chip in metal cutting, causing tools wear, cutting deformation, and tools life decrease [1]. In order to improve the lubrication in the cutter-chip contact area and reduce tools wear, the cutting fluid is widely used [2]. Cutting fluids have a positive effect on reducing tool wear, improving surface quality and increasing production efficiency by lubricating the cutting contact area between the cutter and the workpiece [3]. Studies have shown that capillary action is considered to be the mechanism of penetration of cutting fluid into the contact area between cutter and chip [4]. The lubrication of the cutting fluid is weakened due to its difficulty of penetrating into the cutter-chip interface because of extremely high normal stress in the cutting zone. Therefore, in order to make cutting fluid better perform the lubrication, the following contents are studied: the type of the cutting fluid [5], the supply pressure of the cutting fluid [6–9], and different substances added to the cutting fluid [10–14]. For example, Xavior et al. [5] conducted a test for cutting austenitic stainless steel in the case where three kinds of cutting fluids were separately provided. The test revealed that coconut oil can be more conducive to tool surface lubrication than the other two cutting fluids. Ayed [6] suggested that increasing the injection pressure of cutting fluids could promote tool lubrication, extend cutting tools life, and reduce tool wear by machining Ti17 titanium alloy with carbide tools. Ehsan et al. [11] completed the test of cutting hardened AISI 1045 steel under the lubrication provided by water-mixed vegetable oil which was doped with quantitative antibacterial agent and essence. Results showed that the machined surface quality and the cutting performance were improved. Anuj [12] researched the effect of alumina-graphene composite nanoparticles on the lubricating properties of cutting fluids by turning AISI 304 steel. Results showed that the tool flank wear and node temperature were both reduced because of the application of composite nano-lubricants.

Recently, surface texture has been used to improve the lubrication between friction surfaces, and the textured surface significantly reduced friction and surface damage compared to

✉ Jianxin Deng
jxdeng@sdu.edu.cn

[1] Key Laboratory of High Efficiency and Clean Mechanical Manufacture of MOE, Department of Mechanical Engineering, Shandong University, Jinan 250061, People's Republic of China

Table 1 Properties of YS8 cemented carbide tool materials

Composition (wt%)	Density (g/cm^3)	Hardness (HRA)	Flexural strength (MPa)	Young's modulus (GPa)	Poisson's ratio	Thermal expansion coefficient (10^{-6}/K)
WC + TiC + Co	13.9	92.5	1720	550	0.27	5.5

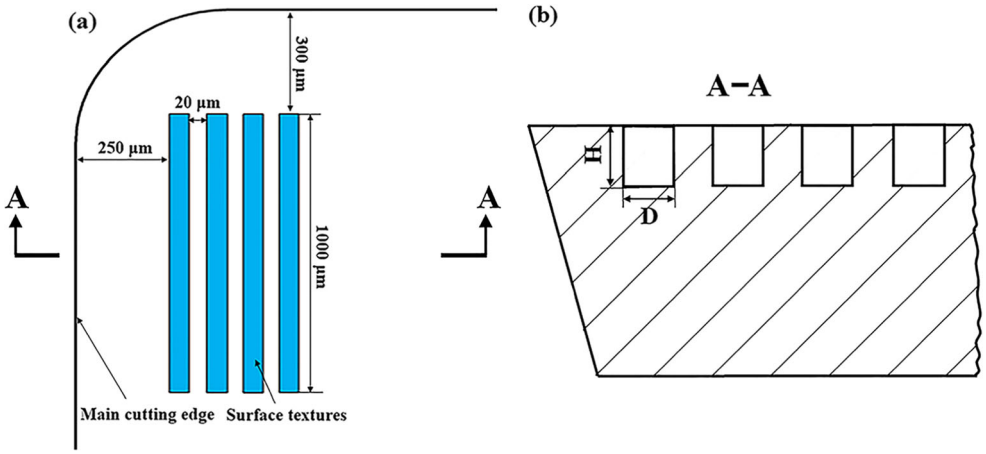

Fig. 1 Diagrammatic sketches of micro-textured tool. (**a**) The rake-face of the textured cutter. (**b**) Sectional view of textured rake-face

untreated surfaces. The main applications of surface texture include bearings, automotive piston rings, wet clutches, and seals [15–24]. The advantage of surface texture to reduce friction is mainly attributed to the following mechanisms: The actual contact area of the friction pair is reduced by texture; the lubricant is stored in the texture space; and the wear debris is collected by the texture space and the formation of fluid dynamic lubrication [25–27]. For example, Sorin-Cristian [15] processed the texture of different shapes and directions on the friction surface of the bearing and studied its influence

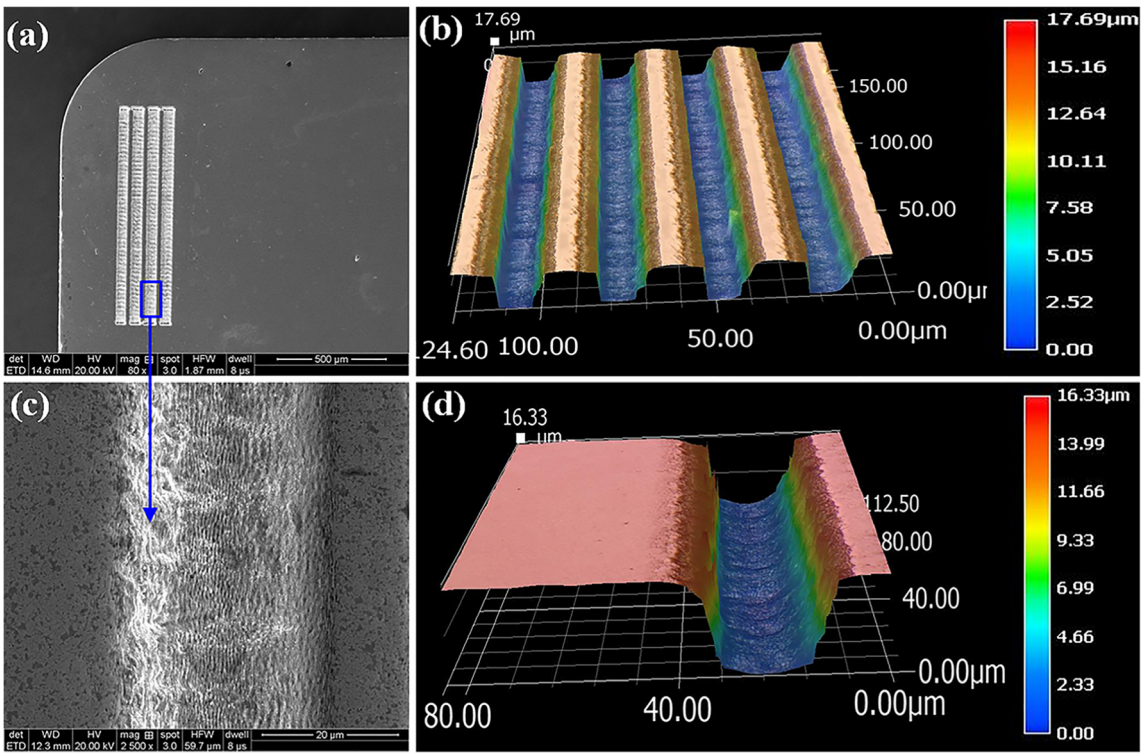

Fig. 2 Photomicrographs of micro-textures. (**a**), (**c**) SEM plane topography. (**b**), (**d**) Three-dimensional appearance

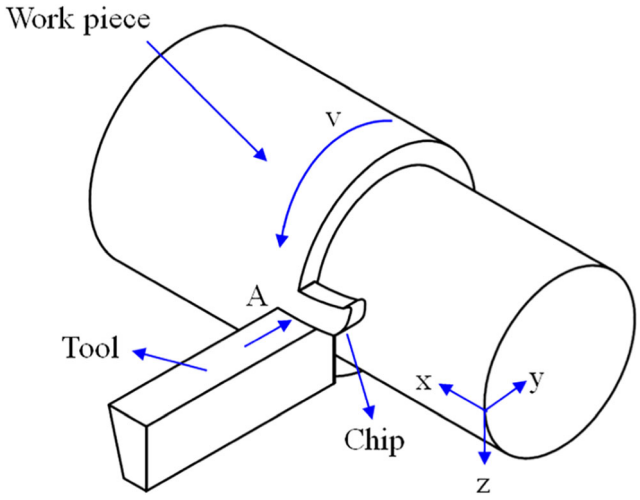

Fig. 3 Diagrammatic sketch of turning

on the friction performance of the bearing using the developed friction instrument. Results revealed that friction and wear could be reduced by the surface texture. Shen et al. [23] used pulsed laser to form five types of oil pockets with varying pocket densities and depths on the surface of piston ring and carried out friction test with them. Results suggested that surface textures can significantly reduce the dynamic friction coefficients. Some researchers have processed the texture on the tool surface to get the optimal cutter friction conditions [28–31]. For example, micro-cylindrical holes were machined on cutter rake-face and filled by WS_2 solid lubricant, and the micro-textures made the tool friction performance better [32]. However, there are currently few studies on the micro-texture effect on the lubrication of cutting fluids.

In the paper, straight micro-textures with a different value of microgroove width were prepared by femtosecond laser on YS8 carbide cutters rake-face. Cutting tests were performed with micro-textured tools of different groove widths and an un-textured cutter under full cutting fluid. Cutting forces and wear of the cutter in interface between the tool and the chip were analyzed. The effect of the micro-texture with different groove widths on the lubrication of cutting fluid was studied.

2 Experimental procedures

2.1 Preparation of micro-textured tools

In this experiment, tool material was designated as YS8 cemented carbide. Table 1 shows the basic properties of YS8 cemented carbide. The shape of the cutting tool was a rectangular solid; its length, width, and height were 16 mm, 16 mm, and 5 mm. Micro-textures with different rectangular groove widths (10 μm, 30 μm, and 50 μm) on the rake-face of these

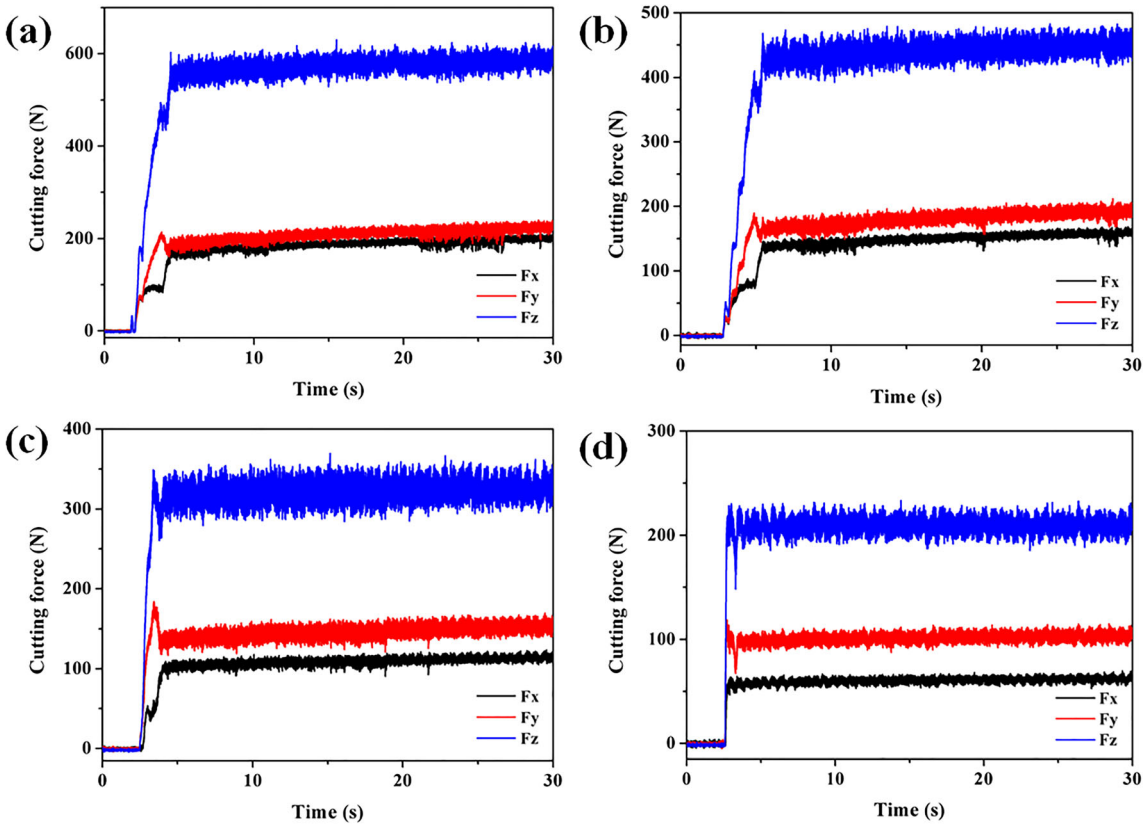

Fig. 4 Variation of cutting force of different cutters in wet turning (cutting speed 150 m/min). (**a**) UTT. (**b**) MTT-1. (**c**) MTT-2. (**d**) MTT-3

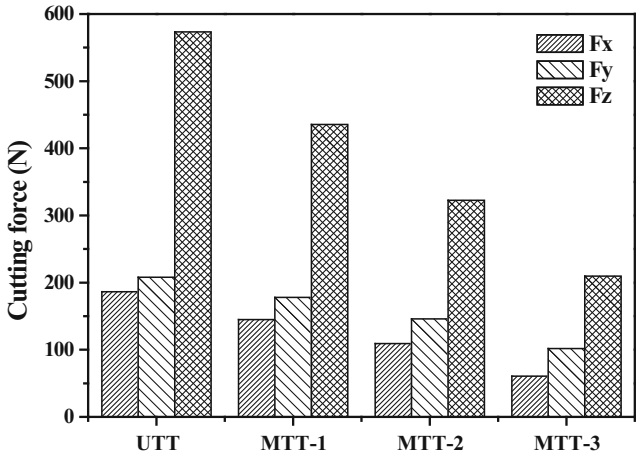

Fig. 5 Cutting force of different cutters during stable cutting in wet turning (cutting time 3.5 min, cutting speed 150 m/min)

cutters were made according to the processing requirements shown in Fig. 1 by femtosecond laser (type: Coherent-Ti gem). The schematic view of the cross section of micro-textured tools is shown in Fig. 1(b). The three micro-textured tools are only different in texture width (D). The height (H) of all micro-textures is 16 μm. For simplicity of description, the three micro-textured tools are named as follows: (1) Micro-textured cutter with groove width of 10 μm is named MTT-1, (2) micro-textured cutter with groove width of 30 μm is named MTT-2, and (3) micro-textured cutter with groove width of 50 μm is named MTT-3. The main cutting edge is paralleled with line of the texture. Figure 2 shows the scanning electron microscope (SEM) and three-dimensional micrograph of the micro-texture on cutter rake-face.

2.2 Cutting tests

The experiment was conducted by cutting H13 hot die steel on a CA6140 lathe. The cutting geometry parameters were rake angle $\gamma_o = -5^\circ$, side cutting edge angle $K_r = 45^\circ$, and inclination angle

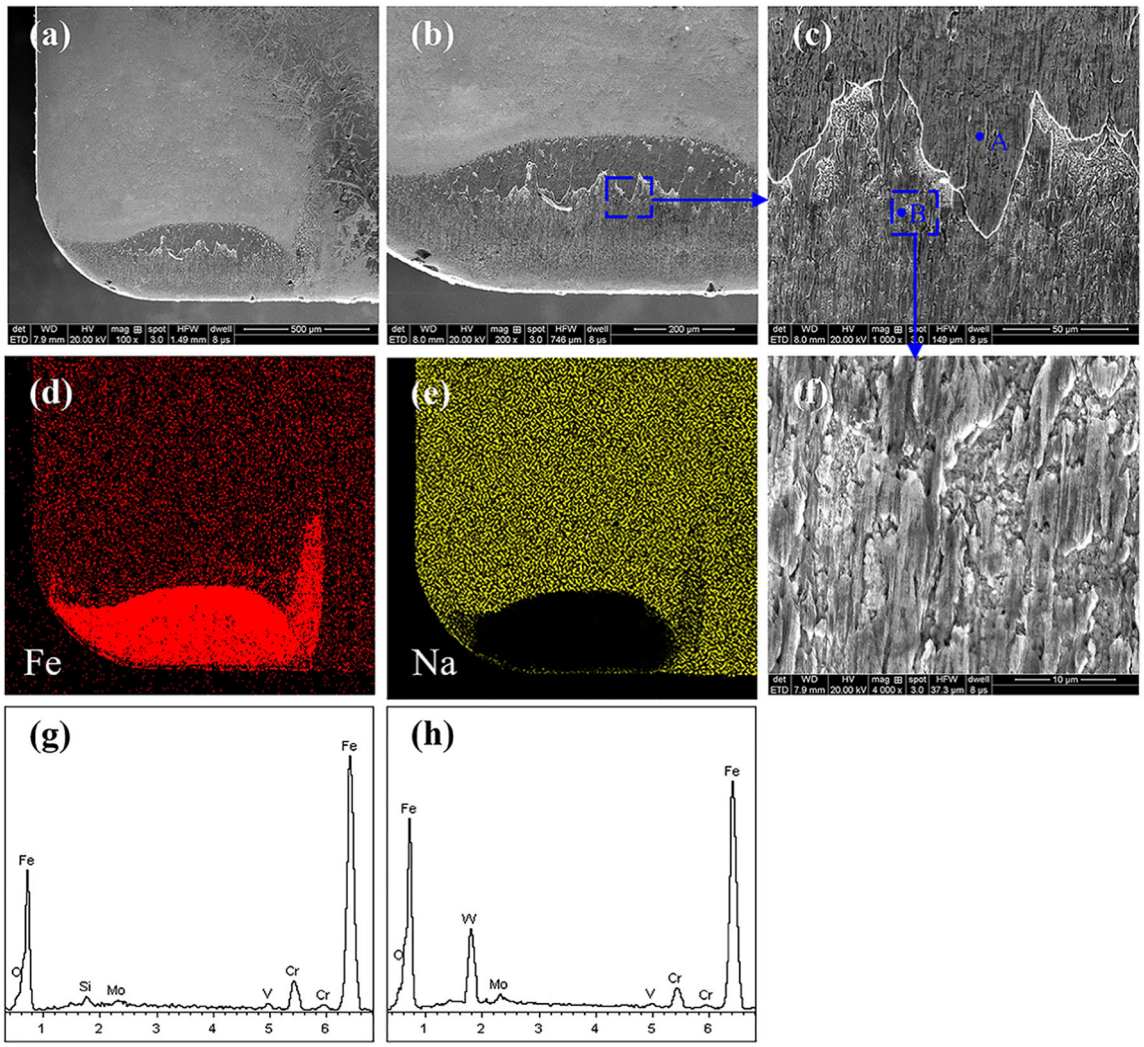

Fig. 6 Micrographs of the UTT cutter rake-face after wet cutting (cutting time 3.5 min, cutting speed 150 m/min). (**a**)–(**c**), (**f**) SEM images of the worn surface. (**d**) Distribution map of Fe element. (**e**) Distribution map of Na element. (**g**) EDX analysis of point A. (**h**) EDX analysis of point B

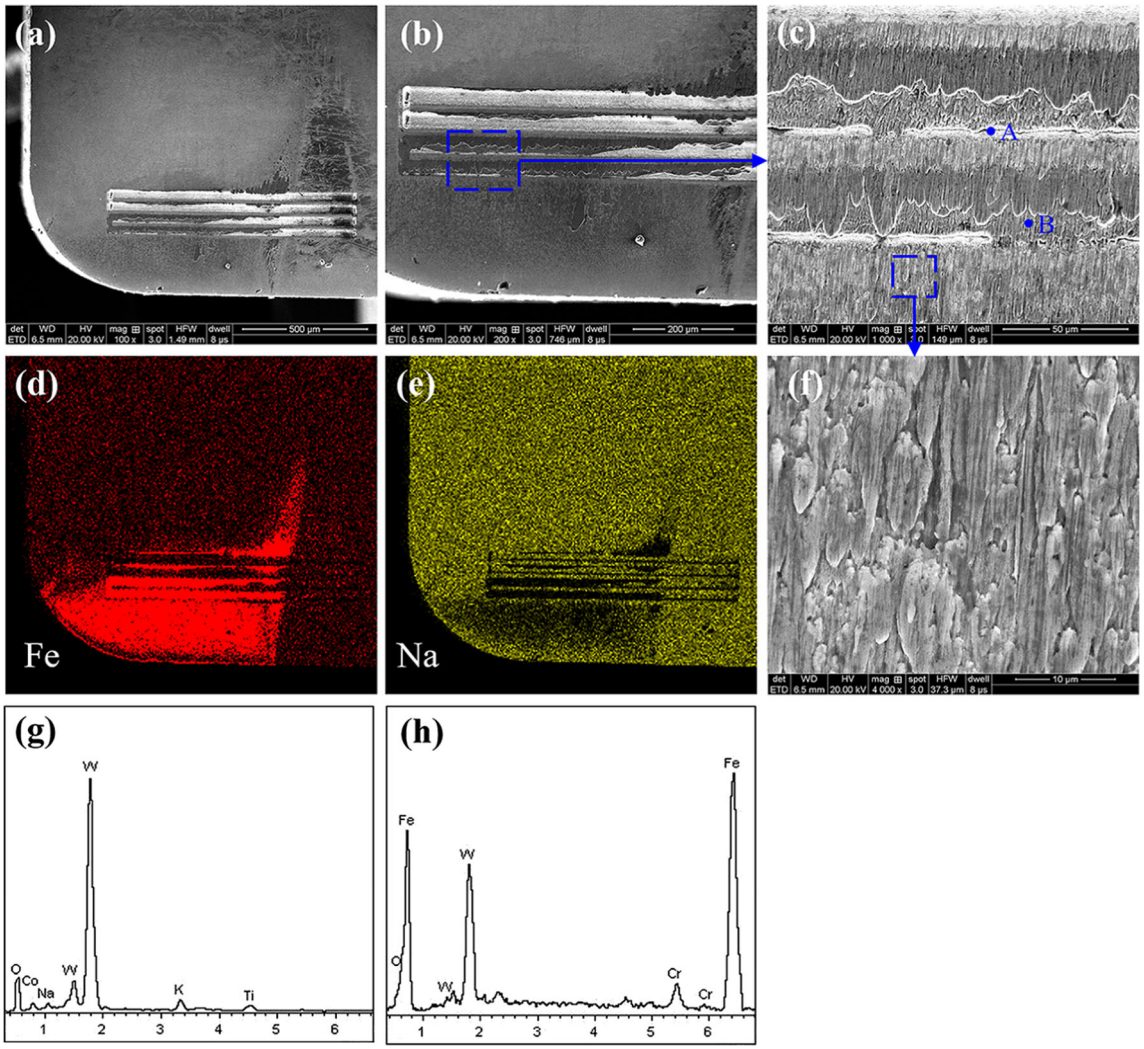

Fig. 7 Micrographs of the MTT-1 cutter rake-face after wet cutting (cutting time 3.5 min, cutting speed 150 m/min), (**a**)–(**c**), (**f**) SEM images of the worn surface. (**d**) Distribution map of Fe element. (**e**) Distribution map of Na element. (**g**) EDX analysis of point A. (**h**) EDX analysis of point B

$\lambda_s = 0^\circ$. The chemical composition of the workpiece (H13 hot die steel) with a diameter of 110 mm is Si 0.96%, Mn 0.38%, C 0.4%, Cr 4.82%, Ni 0.18%, Mo 1.44%, and V 0.92%; and the balance is Fe. The heat-treated H13 hot die steel is of 55 ± 2 HRC in hardness. Micro-textured inserts MTT-1, MTT-2, and MTT-3 were used in this cutting experiment. Moreover, for comparison, the cutting test was also carried out with the untextured cutter which is named UTT. Each turning tool has the same cutting quantity: cutting speed $v = 150$ m/min, cut depth $a_p = 0.5$ mm, and feed rate $f = 0.198$ mm/r. The entire process of all tests was under the emulsified cutting fluids (solcut oil-V600, DOMINO Co. Ltd.). The rate of continuous supply of cutting fluids was 11.2 L/min at one side of the cutter rake-face (pointing A) as displayed in Fig. 3. It took 3.5 min for each cutting. To ensure the reproducibility of results, all tests on each cutting tool were performed thrice and the average values were presented.

Cutting force was recorded with a data logger connected to a KISTLER 9275A piezoelectric quartz dynamometer. The wear morphologies of tested cutter rake-face were surveyed by the scanning electron microscope (QUANTA FEG 250, FEI Inc., USA). Similarly, the chemical composition of the wear zone was obtained by energy-dispersive X-ray spectroscopy (EDX, Oxford Instruments Inc., UK). In addition, the contour of the rake-face of worn cutter and metal structure of cross section of chips were observed using an optical microscope (VK-X200, KEYENCE (China) Co., Ltd.).

3 Results and discussion

3.1 Cutting forces

Figure 4 shows the evolution of the components in the three directions of cutting forces with UTT, MTT-1, MTT-2, and MTT-3 cutters in wet turning at 150 m/min. The cutting force increased sharply at the beginning of the

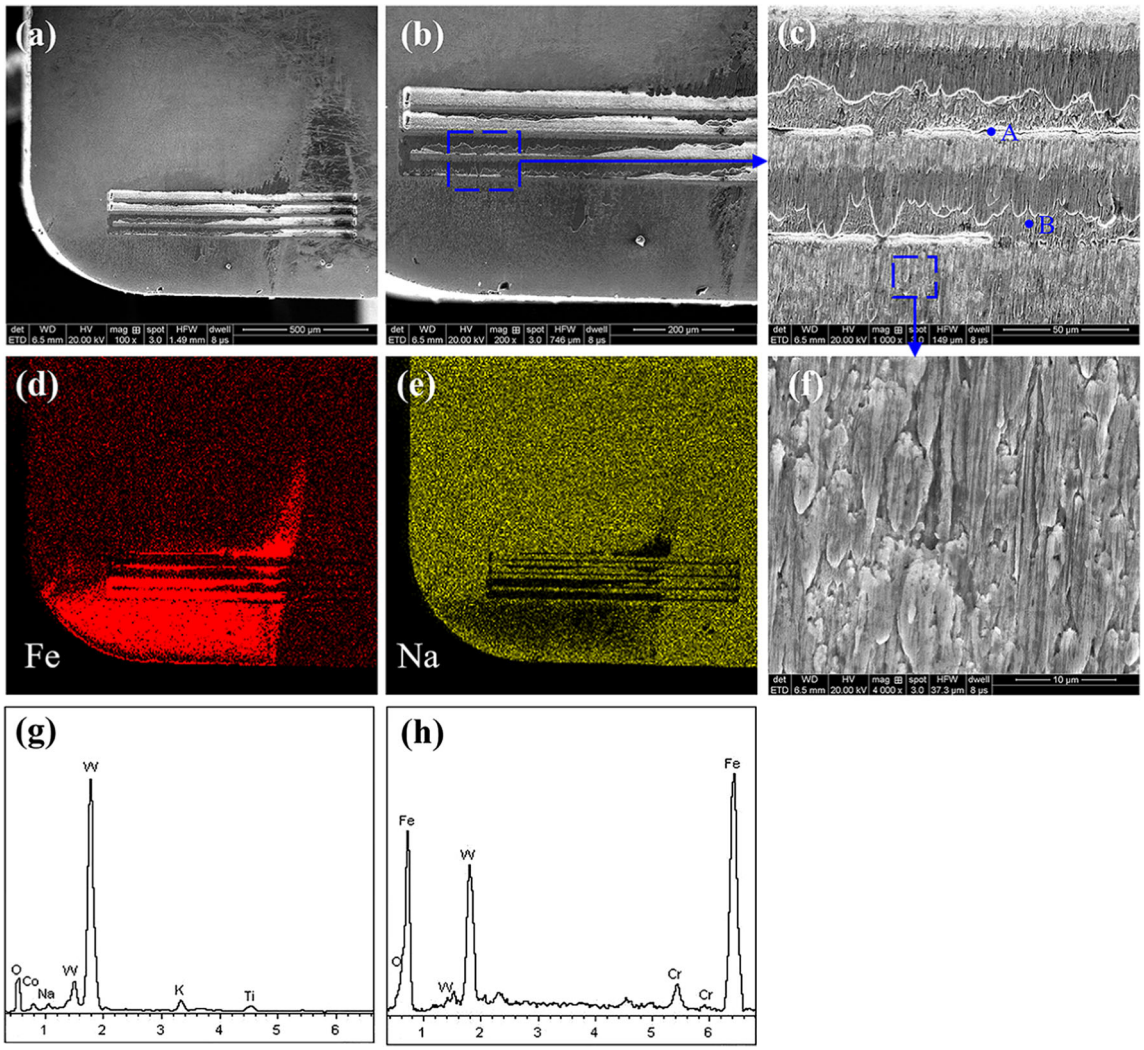

Fig. 8 Micrographs of the MTT-2 cutter rake-face after wet cutting (cutting time 3.5 min, cutting speed 150 m/min). (**a**)–(**c**), (**f**) SEM images of the worn surface. (**d**) Distribution map of Fe element. (**e**) Distribution map of Na element. (**g**) EDX analysis of point A. (**h**) EDX analysis of point B

cutting and then became relatively stable. Among them, the over-excursion process of textured MTT-3 cutter is the fastest and most stable. This is because the cutting fluid that penetrates into the cutting zone increases as the texture size increases. The more cutting fluid, the better the lubrication of the cutting zone. Therefore, the tool MTT-3 with the largest texture size was best lubricated and reached the stable cutting state as early as possible.

Figure 5 plots the average of the three components (F_x, Fy, and F_z) of cutting forces of the four tools at a stable wet cutting of 150 m/min. Under the same conditions, the three cutting forces of the traditional non-texturing tool UTT are significantly higher than the textured cutters. Main cutting force F_z of micro-textured cutters (MTT-1, MTT-2, and MTT-3) was reduced by 24.0%, 43.7%, and 63.4%, respectively, compared to un-textured cutter (UTT). Similarly, radial thrust force Fy was reduced by 14.4%, 29.8%, and 51.1%, and axial thrust force F_x was reduced by 22.2%, 41.4%, and 67.4%.

3.2 Cutter worn surfaces

SEM images and EDX analyses of worn UTT tool rake-face after cutting for 3.5 min in speed of 150 m/min with providing cutting fluid lubrication are shown in Fig. 6. The crater wear on the cutting area of UTT cutter rake-face is clearly identified as displayed in Fig. 6(a), (b). Obvious and severe adhesion can be found by the magnified micrographs (Fig. 6(c)). A large number of plows are clearly visible on the wear trace by further magnification of the UTT tool wear surface (Fig. 6(f)), which indicates that there is severe abrasive wear on tool rake-face. EDX analyses of points A and B in cutting zone are shown in Fig. 6(g), (h), respectively. The results show that the adhesion of the edge region (point A) of the crater wear does not contain any elements in the tool material. Instead, all of these elements come from the workpiece. At the same time, the middle part (point B) of the crater

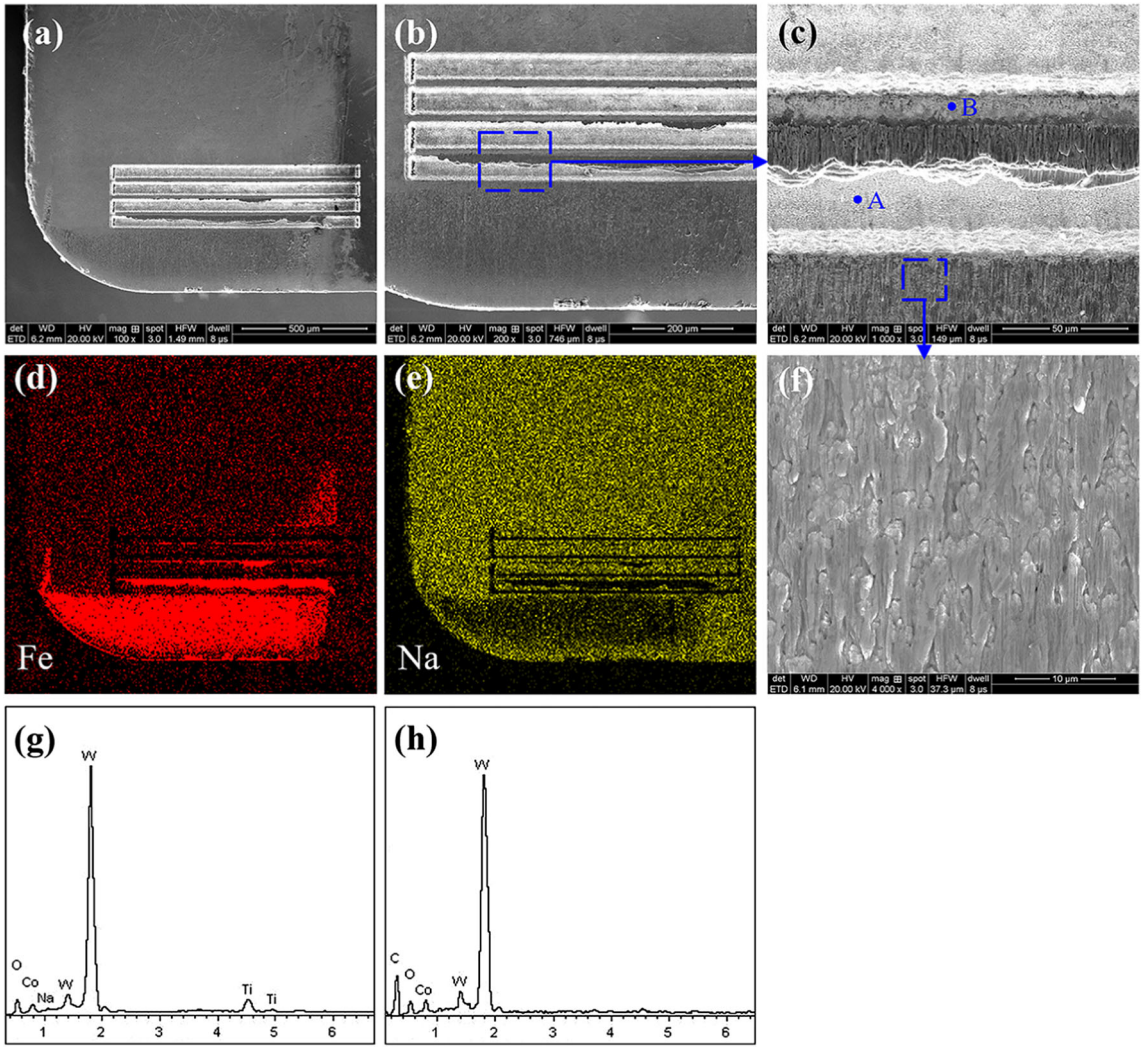

Fig. 9 Micrographs of the MTT-3 cutter rake-face after wet cutting (cutting time 3.5 min, cutting speed 150 m/min). (**a**)–(**c**), (**f**) SEM images of the worn surface. (**d**) Distribution map of Fe element. (**e**) Distribution map of Na element. (**g**) EDX analysis of point A. (**h**) EDX analysis of point B

wear contains both the elements in the tool and the workpiece. EDX distribution pattern of Fe element of the UTT tool rake-face is shown in Fig. 6(d), and the whole cutting area of the cutter is covered by Fe element. The above results indicate that there is severe adhesion wear in the cutting area. As mentioned above, the material of cutter and workpiece used during turning process does not contain Na element. Nevertheless, the emulsified cutting fluid contains Na element. Therefore, the Na element was observed to determine the penetration of the cutting fluid in the cutting zone. EDX distribution pattern of Na element on UTT cutter rake-face is shown in Fig. 6(e). There is almost no Na element in the entire cutting zone, indicating that little cutting fluid penetrated into cutter-chip contact area during the UTT tool cutting.

SEM images and EDX analyses of worn MTT-1 tool rake-face after cutting for 3.5 min in speed of 150 m/min with providing cutting fluid lubrication are shown in Fig. 7. No obvious crater wear is found on the cutting surface of the MTT-1 tool (Fig. 7(a), (b)). A small amount of adhesion in the MTT-1 tool cutting zone is shown in high magnification image (Fig. 7(c)) compared to the UTT tool. It is worth noting that the adhesion of the MTT-1 tool is concentrated in the micro-grooves so that micro-textures close to nose of turning tool are completely or partially filled. The wear surface (Fig. 7(f)) with shallow plows is smoother than that of the UTT cutter, which indicates that there is smaller hard spot wear in the cutting zone of the MTT-1 tool. Figure 7(g), (h) shows the EDX analyses of points A and B on the cutter rake-face, respectively. The results show that the adhesion in the micro-groove is mainly derived from the workpiece material. At the same time, the unfilled micro-groove contains Na element in addition to tool material elements. This indicates that the cutting fluid flowed along the microgrooves into the cutter-chip interface during the turning of MTT-1 tool,

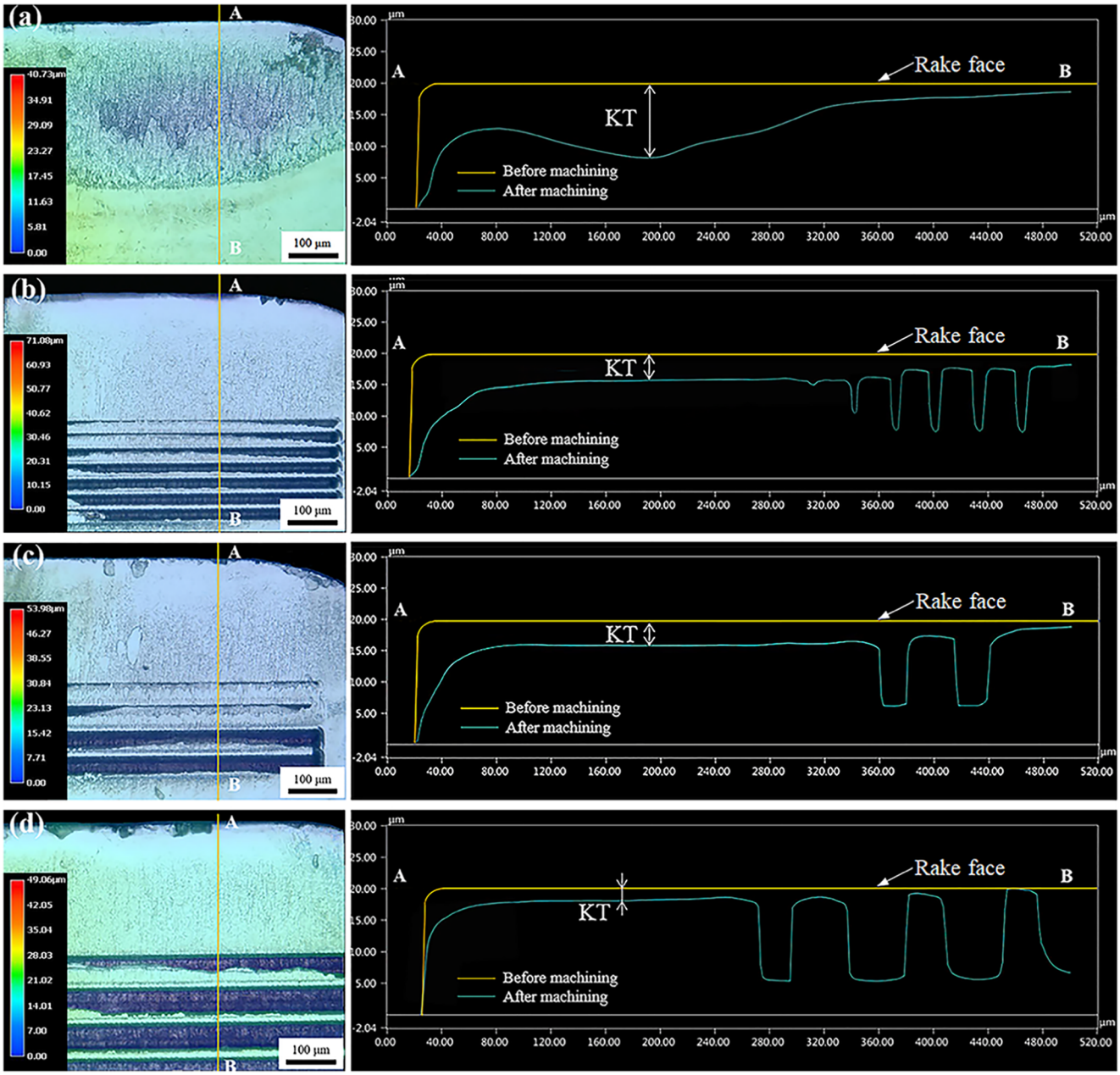

Fig. 10 Three-dimensional profiles (left) and cross section profiles (right) of the worn cutters rake-face after wet turning (cutting speed 150 m/min, cutting time 3.5 min). (**a**) UTT. (**b**) MTT-1. (**c**) MTT-2. (**d**) MTT-3

which greatly improved lubrication of cutting fluid. The distribution of Fe element shown in Fig. 7(d) further indicates that the workpiece material did not adhere to the entire cutting zone like the UTT tool but mainly adhered to the inside of the microgroove. The presence of Na element in cutter-chip contact area as shown in Fig. 7(e) further demonstrates that the cutting fluid successfully penetrated into the cutting zone during the cutting process.

SEM images and EDX analyses of worn MTT-2 tool rake-face after cutting for 3.5 min in speed of 150 m/min with providing cutting fluid lubrication are shown in Fig. 8. The MTT-2 tool is similar to the MTT-1 tool. The cutting fluid penetrated into cutting contact zone, and micro-grooved textures were also filled with workpiece material in whole or in part. However, the wear of MTT-2 cutter was significantly smaller compared to that of UTT cutter.

SEM images and EDX analyses of worn MTT-3 tool rake-face after cutting for 3.5 min in speed of 150 m/min with providing cutting fluid lubrication are shown in Fig. 9. The wear of MTT-3 tool rake-face was smaller and lighter than that of the other three tools (UTT, MTT-1, and MTT-2) as shown in Fig. 9(a), (b). The

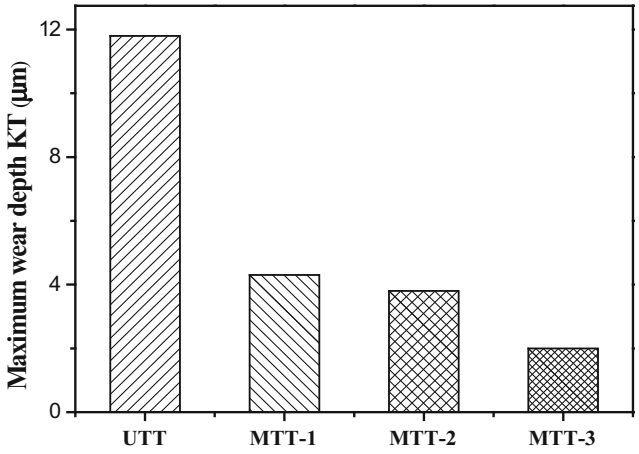

Fig. 11 Maximum wear depth of the worn cutters rake-face after wet turning (cutting speed 150 m/min, cutting time 3.5 min)

plowing marks were hardly seen in the enlarged view of the worn surface of MTT-3 as shown in Fig. 9(f). Moreover, it can be seen in conjunction with Fig. 9(c), (d) that only little working parts material adhered to a micro-textured groove closest to nose of turning tool, and the remaining micro-texture was hardly affected. The EDX analysis shown in Fig. 9(h) shows that the element in the workpiece material is not contained at point B in Fig. 9(c), which indicates that there is no adhesion of the workpiece on the tool cutting surface between the micro-textured grooves. The EDX analysis shown in Fig. 9(g) shows that Na element is present in the micro-groove at point A, suggesting that the cutting fluid flowed into the micro-trench in cutter-chip contact zone. The above inference is confirmed by the distribution of the Na element in Fig. 9(e). It is noteworthy that even the micro-grooved texture with the most adhesive is only partially filled and not completely blocked. This allows the cutting fluid continuously to flow along the micro-grooved texture into the cutting zone to provide lubrication at the cutter-chip interface during cutting with the MTT-3 tool.

3.3 Profiles of the worn rake-faces

Surface topography and the cross section contour of worn cutter rake-face were observed using an optical microscope after wet cutting (cutting speed 150 m/min, cutting time 3.5 min) as shown in Fig. 10. There is a noticeable crater profile on worn UTT cutter rake-face (Fig. 10(a)). Correspondingly, no obvious worn concave profile was found on the wear rake-face of micro-grooved cutters (MTT-1, MTT-2, and MTT-3), and their average wear depth was significantly smaller compared to non-textured UTT cutter (Fig. 10(b)–(d)). In addition, three micro-textures with different groove widths were in

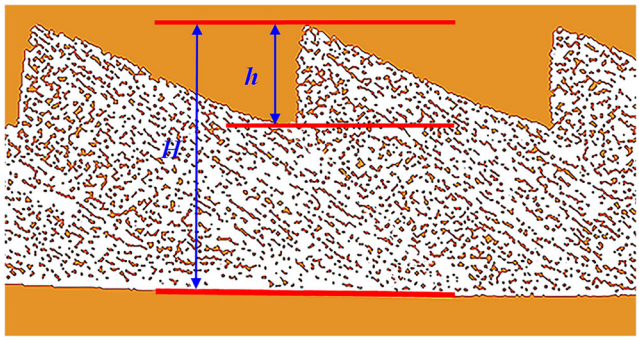

Fig. 12 Schematic diagram of the serrated chip

various degrees of completeness after the same cutting test as shown in Fig. 10. The partial contours of the two micro-textures with groove widths of 10 μm and 30 μm can be seen on the far side from the cutting edge (Fig. 10(b), (c)). The contour of the micro-texture with a groove width of 50 μm was found to be hardly damaged (Fig. 10(d)), which provided sufficient space for cutting fluid to flow smoothly into cutter-chip contact zone.

Maximum wear depth of tested cutter rake-face is shown in Fig. 11. Maximum wear depth of micro-textured tools with groove widths of 10 μm, 30 μm, and 50 μm (MTT-1, MTT-2, and MTT-3) was reduced by 63.8%, 68.1%, and 83.2%, respectively, compared to un-textured cutter (UTT).

3.4 The cutting shear angle

Since the shear angle is inversely proportional to the friction coefficient in cutter-chip contact zone, the shear angle Φ can characterize the lubricity of the cutting zone [33]. The shear angle Φ can be expressed by the equation [34, 35]:

$$\Phi = \arctan\frac{\cos\gamma_o}{\xi - \sin\gamma_o} \tag{1}$$

where Φ is the shear angle, ξ is the chip-thickness ratio, and γ_o is the rake angle. The chip-thickness ratio ξ can be calculated by the equation:

$$\xi = \frac{a_{ch}}{a_c} \tag{2}$$

where a_c is the undeformed chip-thickness that can be obtained as $a_c = f \times \sin K_r$ (where f and K_r are certain), a_{ch} is the deformed chip-thickness that can be expressed by the equation [36]:

$$a_{ch} = H - \frac{h}{2} \tag{3}$$

where H and h marked in the schematic diagram Fig. 12 could be obtained by measuring the geometry of the serrated chip as shown in Fig. 13.

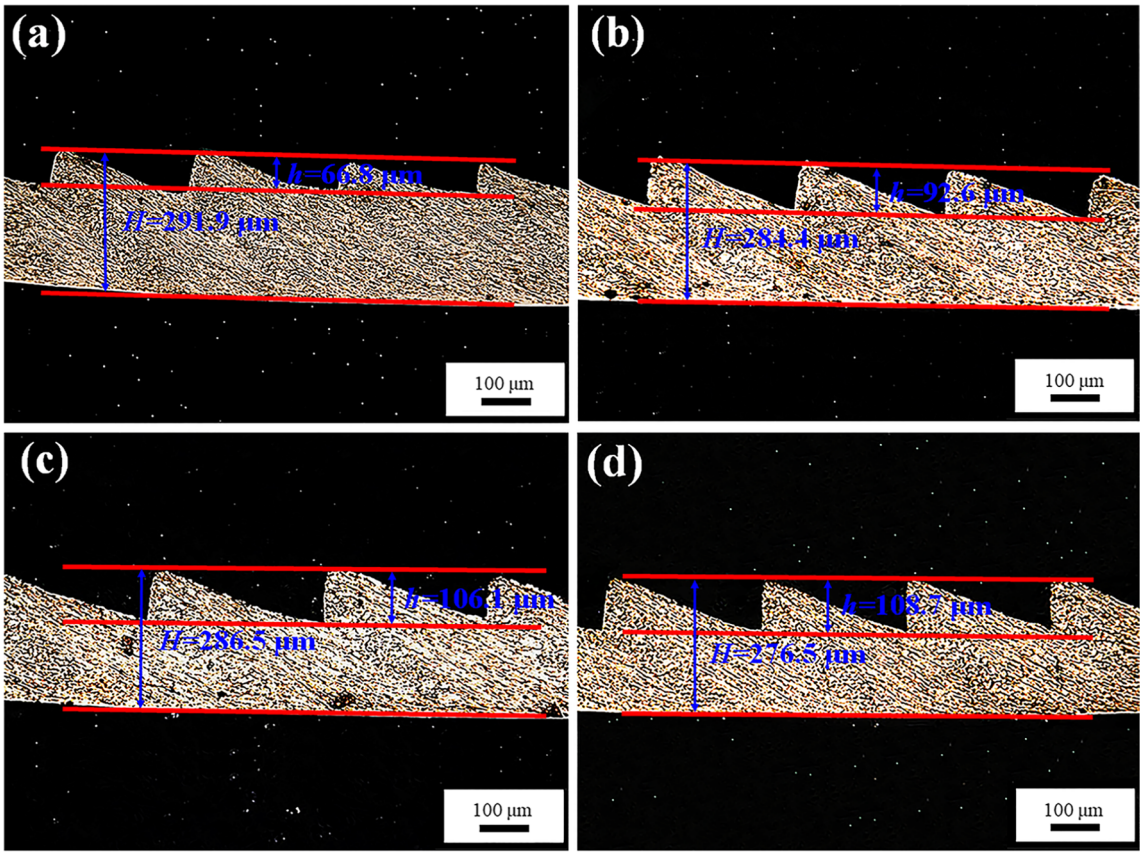

Fig. 13 Chip morphologies for the worn tools after wet cutting (cutting speed 150 m/min, cutting time 3.5 min). (**a**) UTT. (**b**) MTT-1. (**c**) MTT-2. (**d**) MTT-3

Chip morphologies for the worn tools after wet cutting (cutting speed 150 m/min, cutting time 3.5 min)—(a) UTT, (b) MTT-1, (c) MTT-2, and (d) MTT-3—are shown in Fig. 13. The shear angles corresponding to the four cutting inserts are shown in Fig. 14. The results show that the shear angles of textured cutters were larger than that of the untextured insert. The shear angle of the MTT-1, MTT-2, and MTT-3 increased by 7.8%, 10.0%, and 14.6% compared to that of the UTT, respectively.

3.5 The friction coefficient between cutter and chip

The friction coefficient between cutter and chip can be expressed by the equation [37]:

$$\mu = \tan(\beta) \tag{4}$$

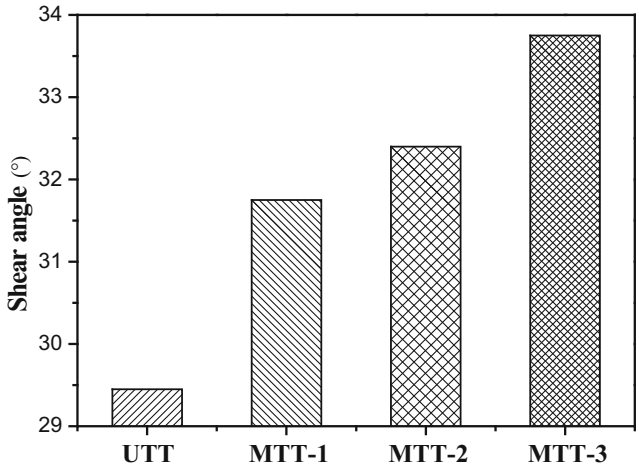

Fig. 14 Shear angle of different cutting tools in wet turning (cutting time 3.5 min, cutting speed 150 m/min)

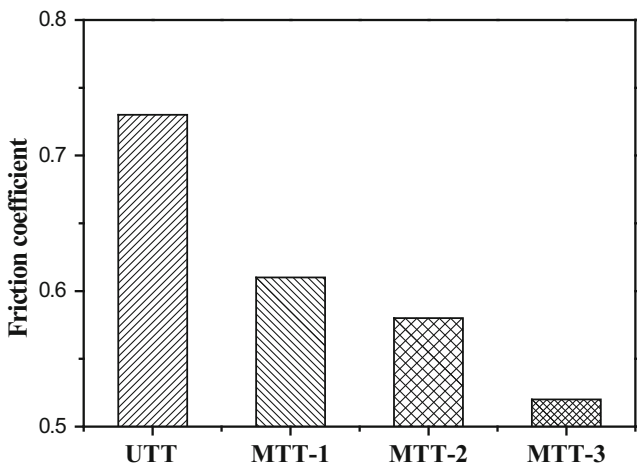

Fig. 15 Friction coefficient of the cutter-chip interface in wet turning (cutting time 3.5 min, cutting speed 150 m/min)

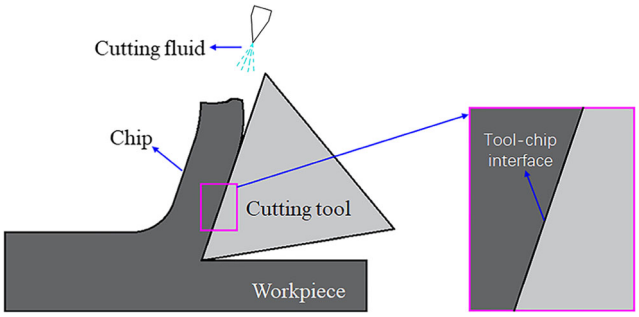

Fig. 16 Diagrammatic sketches of the friction interface of conventional tool (UTT)

where is the friction angle that could be expressed by the formula:

$$\beta = \frac{\pi}{2} + \gamma_o - 2\Phi \tag{5}$$

where γ_o is the rake angle and Φ determined by the previous section is the shear angle.

The friction coefficient between cutter and chip of different cutting tools in wet cutting is shown in Fig. 15. The friction coefficient of textured tools is smaller compared to the non-textured tool. The value of the friction coefficient for MTT-1, MTT-2, and MTT-3 is reduced by 16.4%, 20.5%, and 28.8% compared to the UTT, respectively.

4 Discussion

In this paper, micro-textures were prepared on the carbide inserts rake-face, and their effects on the penetration and lubrication of the cutting fluid in wet cutting H13 hot die steel were studied. The micro-textured tools can greatly improve the penetration and lubrication of cutting fluids. The textured tools with micro-grooves with a width of 50 μm (MTT-3) had the best effect as shown in Figs. 9 and 10. The corresponding mechanisms were discussed as follows.

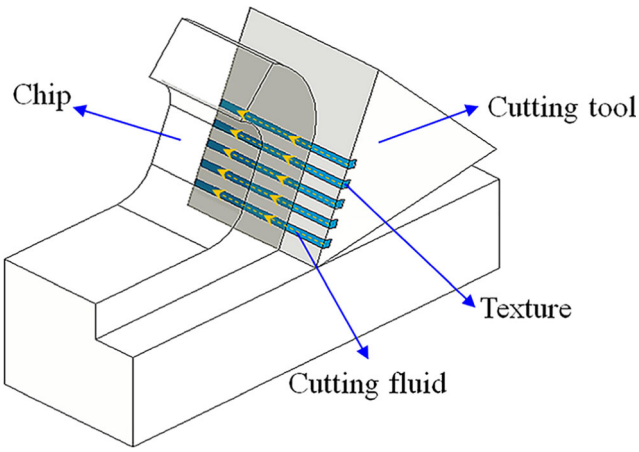

Fig. 17 Schematic diagram of cutting fluid flowing into the cutting zone on the textured tool rake-face

The reduction of friction between cutter and chip depends on the lubrication of the influent cutting fluid. However, only little cutting fluid penetrates into cutter-chip contact area for traditional cutting tools, and the infiltration process of the cutting fluid is not well understood [38].

Figure 6(e), (g), (h) shows that the cutting fluid almost did not flow into the UTT cutter cutting zone. The main reason is that the friction between cutter and chip is very severe. Figure 16 schematically shows the tool-chip contact condition of conventional tool (UTT) without surface gaps. The tool material is in tight contact and even involves atomic bonding with the workpiece material due to the intense stress and strain in turning process. This severe friction condition results in little or no lubricating fluid penetrating into the contact area on the cutter rake-face [39]. The workpiece material may adhere to the tool cutting surface where it is not lubricated by the cutting fluid. The adhesive material will carry some of the tool material away from the cutter rake-face when the adhesion reaches a certain level. This repeated adhesion may result in the friction loss of the tool materials. For the above reasons, severe adhesion showed in the wear morphology (as shown in Fig. 6(a)–(c)) and obvious wear (as shown in Fig. 10(a)) of traditional tool (UTT) is understood.

Figure 7 shows wear photomicrographs of the textured MTT-1 cutter rake-face after the cutting lubricated by the cutting fluid (cutting time 3.5 min, cutting speed 150 m/min). The distribution of Na element shown in Fig. 7(e) meant that the lubricating fluid penetrated into contact zone between cutter and chip. The EDS elemental analysis of point A (Fig. 7(c)) in the micro-grooved texture shown in Fig. 7(g) showed the presence of the Na element, which further verified that the lubricating fluid flowed into the cutting zone through the micro-textures.

The following explains how the lubricating fluid penetrated into the cutter-chip contact zone through micro-textures. The ability of the penetration of the cutting fluid mainly depends on the micro-path on cutter rake-face [40]. Godleviski [41] attributed the penetration of the cutting fluid to the capillary action at the cutting interface. They created a model of a single interface capillary and divided the capillary action of cutting fluid into three stages: (a) fluid phase penetration, (b) micro-droplets vaporization and explosion, and (c) lubrication interface by gas phase. The concept of infiltration in the above model can be extended to micro-textured tools. Negative pressure can be created in the micro-grooves because of the relative movement of cutter and chip. The pressure in the micro-textured groove is lower than the external pressure, which causes the cutting fluid to actively flow into the

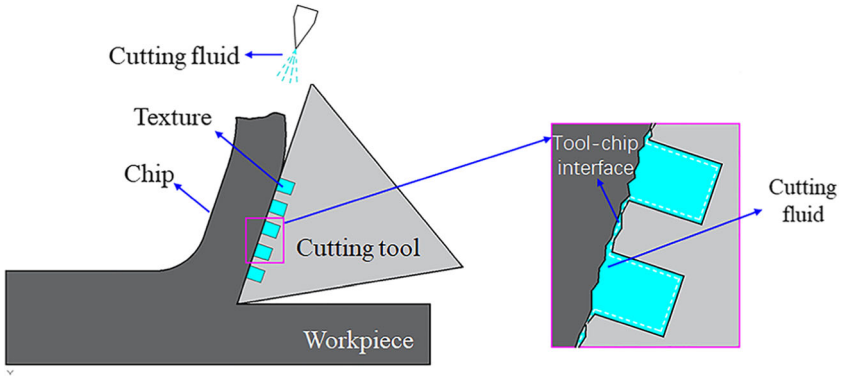

Fig. 18 Diagrammatic sketches of the friction interface of the textured tool (MTT-3)

micro-groove. The cutting fluid can flow along the micro-groove into the contact area between cutter and chip as displayed in Fig. 17. In addition, micro-textures can function as reservoirs and the stored cutting solution can be continuously smeared on the interface between cutter and chip forming a lubricating film. It is the penetration of cutting fluid that improves friction properties in the cutting contact zone. The mechanism of the penetration lubrication of the cutting fluid for MTT-2 cutter is similar to that of MTT-1 tool.

Figure 9 shows photomicrographs of the textured MTT-3 cutter rake-face after the cutting lubricated by the cutting fluid (cutting time 3.5 min, cutting speed 150 m/min). The distribution of Na element shown in Fig. 9(e) meant that the lubricating fluid penetrated into contact zone between cutter and chip. The EDS elemental analysis of point A (Fig. 9(c)) in the micro-grooved texture showed the presence of the Na element shown in Fig. 9(g), which further verified that the lubricating fluid flowed into the cutting zone through the micro-textures. In fact, the smaller the texture size, the greater the pressure applied by the outside world required for the cutting fluid to penetrate into the cutting zone. In addition, the smaller the texture size, the greater the frictional loss of the cutting fluid in the textured groove. Therefore, the amount of cutting fluid that penetrates into the smaller size texture is limited. Correspondingly, the larger size of the micro-texture could increase the permeability of the lubricating fluid [42]. Therefore, the cutting fluid can flow continuously into the cutting zone of MTT-3 cutter through the completely unimpeded micro-grooved texture. Figure 18 shows schematically the formation of a layer of lubricating film between cutter and chip with sufficient penetration of cutting fluid. It was the lubricating film that minimized cutting forces, maximum wear depth, and friction coefficient at interface of cutter and chip of MTT-3 tool (as shown in Figs. 5, 11, and 15). Current research reveals that microtextures can promote the penetration lubrication of cutting fluids and reduce cutter wear. The next research will focus on the design of microtextures in terms of arrangement, geometry, and orientation and its mechanism of influence on the penetration of cutting fluids.

5 Conclusions

The surface rectangular grooved micro-textures were fabricated on the rake-face of the YG8 cemented carbide tool by femtosecond laser. The tests of wet cutting H13 hot die steel were performed using textured and conventional tools under fully lubricated conditions. The main conclusions were organized as follows:

1. Three micro-textured rake-face tools with different groove width were successfully processed. The micro-textured cutters significantly enhanced penetration of cutting fluids, reduced cutting forces and rake-face wear, and improved lubrication in the cutter-chip interface compared to conventional tools.
2. The MTT-3 tool with micro-textures with groove width of 50 μm showed the smallest cutting force and wear, and retained the most complete micro-texture profile among the four tested cemented carbide tools.
3. The most important mechanism was found, the cutting fluid was provided with sufficient permeation space by the micro-textures, and the cutting fluid could continuously permeate into the cutting zone through the unimpeded micro-grooved textures.

Funding information This work is supported by the Major Program of Shandong Province Natural Science Foundation (ZR2018ZB0522), National Natural Science Foundation of China (51675311), and Development Plan of Science and Technology of Shandong Province (2017GGX30115).

References

1. Puls H, Klocke F, Lung D (2014) Experimental investigation on friction under metal cutting conditions. Wear 310:63–71
2. Kishawy HA, Dumitrescu M, Ng EG, Elbestawi MA (2005) Effect of coolant strategy on tool performance, chip morphology and surface quality during high-speed machining of A356 aluminum alloy. Int J Mach Tools Manuf 45:219–227
3. Sreejith PS (2008) Machining of 6061 aluminium alloy with MQL, dry and flooded lubricant conditions. Mater Lett 62:276–278

4. DeChiffre L (1981) Lubrication in cutting-critical review and experiments with restricted contact tools. ASLE Trans 24:340–344
5. Xavior MA, Adithan M (2009) Determining the influence of cutting fluids on tool wear and surface roughness during turning of AISI 304 austenitic stainless steel. J Mater Process Technol 209: 900–909
6. Ayed Y, Germain G, Ammar A, Furetb B (2015) Tool wear analysis and improvement of cutting conditions using the high-pressure water-jet assistance when machining the Ti17 titanium alloy. Precis Eng-J Int Soc Precis Eng Nanotechnol 42:294–301
7. Ayed Y, Germain G, Ammar A, Furet B (2013) Degradation modes and tool wear mechanisms in finish and rough machining of Ti17 titanium alloy under high-pressure water jet assistance. Wear 305: 228–237
8. da Silva RB, Machado AR, Ezugwu EO, Bonney J, Sales WF (2013) Tool life and wear mechanisms in high speed machining of Ti–6Al–4V alloy with PCD tools under various coolant pressures. J Mater Process Technol 213:1459–1464
9. Su GS, Guo YK, Song XL, Tao H (2016) Effects of high-pressure cutting fluid with different jetting paths on tool wear in cutting compacted graphite iron. Tribol Int 103:289–297
10. Sartori S, Ghiotti A, Bruschi S (2018) Solid lubricant-assisted minimum quantity lubrication and cooling strategies to improve Ti6Al4V machinability in finishing turning. Tribol Int 118:287–294
11. Shokoohi Y, Khosrojerdi E, Shiadhi BHR (2015) Machining and ecological effects of a new developed cutting fluid in combination with different cooling techniques on turning operation. J Clean Prod 94:330–339
12. Sharma AK, Tiwari AK, Dixit AR, Singh RK, Singh M (2018) Novel uses of alumina/graphene hybrid nanoparticle additives for improved tribological properties of lubricant in turning operation. Tribol Int 119:99–111
13. Chan CY, Lee WB, Wang H (2013) Enhancement of surface finish using water-miscible nano-cutting fluid in ultra-precision turning. Int J Mach Tools Manuf 73:62–70
14. Singh RK, Sharma AK, Dixit AR, Tiwari AK, Pramanik A, Mandal A (2017) Performance evaluation of alumina-graphene hybrid nano-cutting fluid in hard turning. J Clean Prod 162:830–845
15. Vladescu SC, Olver AV, Pegg IG, Reddyhoff T (2015) The effects of surface texture in reciprocating contacts–an experimental study. Tribol Int 82:28–42
16. Vladescu SC, Olver AV, Pegg IG, Reddyhoff T (2016) Combined friction and wear reduction in a reciprocating contact through laser surface texturing. Wear 358(359):51–61
17. Biboulet N, Bouassida H, Lubrecht AA (2015) Cross hatched texture influence on the load carrying capacity of oil control rings. Tribol Int 82:12–19
18. Gachot C, Rosenkranz A, Hsu SM, Costa HL (2017) A critical assessment of surface texturing for friction and wear improvement. Wear 372:21–41
19. Gherca A, Fatu A, Hajjam M, Maspeyrot P (2017) Influence of surface texturing on the hydrodynamic performance of a thrust bearing operating in steady-state and transient lubrication regime. Tribol Int 102:305–318
20. Tala-Ighil N, Fillon M (2015) Surface texturing effect comparative analysis in the hydrodynamic journal bearings. Mech Ind 16:302
21. Wang T, Huang WF, Liu XF, Li YJ, Wang YM (2014) Experimental study of two-phase mechanical face seals with laser surface texturing. Tribol Int 72:90–97
22. Adjemout M, Andrieux A, Bouyer J, Brunetiere N, Marcos G, Czerwiec T (2017) Influence of the real dimple shape on the performance of a textured mechanical seal. Tribol Int 115:409–416
23. Shen C, Khonsari MM (2016) The effect of laser machined pockets on the lubrication of piston ring prototypes. Tribol Int 101:273–283
24. Sudeep U, Tandon N, Pandey RK (2015) Tribological studies of lubricated laser-textured point contacts in rolling/sliding reciprocating motion with investigations of wettability and nanohardness. Tribol Trans 58:625–634
25. Segu DZ, Choi SG, Choi JH, Kim SS (2013) The effect of multi-scale laser textured surface on lubrication regime. Appl Surf Sci 270:58–63
26. Gropper D, Wang L, Harvey TJ (2016) Hydrodynamic lubrication of textured surfaces: a review of modeling techniques and key findings. Tribol Int 94:509–529
27. Ibatan T, Uddin MS, Chowdhury MAK (2015) Recent development on surface texturing in enhancing tribological performance of bearing sliders. Surf Coat Technol 272:102–120
28. Wu Z, Deng JX, Chen Y, Xing YQ, Zhao J (2012) Performance of the self-lubricating textured tools in dry cutting of Ti-6Al-4V. Int J Adv Manuf Technol 62:943–951
29. Deng JX, Lian YS, Wu Z, Xing YQ (2013) Performance of femtosecond laser-textured cutting tools deposited with WS_2 solid lubricant coatings. Surf Coat Technol 222:135–143
30. Xing YQ, Deng JX, Li SP, Yue HZ, Meng R, Gao P (2014) Cutting performance and wear characteristics of Al_2O_3/TiC ceramic cutting tools with WS_2/Zr soft-coatings and nano-textures in dry cutting. Wear 318:12–26
31. Lian YS, Deng JX, Yan GY, Cheng HW, Zhao J (2013) Preparation of tungsten disulfide (WS_2) soft-coated nano-textured self-lubricating tool and its cutting performance. Int J Adv Manuf Technol 68:2033–2042
32. Deng JX, Song WL, Zhang H, Yan P, Liu AH (2011) Friction and wear behaviors of the carbide tools embedded with solid lubricants in sliding wear tests and in dry cutting processes. Wear 270:666–674
33. Enomoto T, Sugihara T (2010) Improving anti-adhesive properties of cutting tool surfaces by nano−/micro-textures. CIRP Ann-Manuf Technol 59:597–600
34. Cheng RY (1992) Principle of metal cutting. China Machine Press, Beijing
35. Shaw MC (1984) Metal cutting principles. Oxford University Press, New York
36. Wang B, Liu Z (2016) Evaluation on fracture locus of serrated chip generation with stress triaxiality in high speed machining of Ti6Al4V. Mater Des 98:68–78
37. Sharma V, Pandey PM (2016) Recent advances in turning with textured cutting tools: a review. J Clean Prod 137:701–715
38. Falco SW, Eduardo DA, Rocha MA (2001) Application of cutting fluids in machining processes. J Braz Soc Mech Sci Eng 23:227–240
39. Trent EM (1988) Metal cutting and the tribology of seizure: I seizure in metal cutting. Wear 128:29–45
40. Godlevski VA, Volkov AV, Latyshev VN, Maurin LN (2010) A description of the lubricating action of the tribo-active components of cutting fluids. Lubr Sci 11:51–62
41. Godlevski VA, Volkov AV, Latyshev VN, Maurin LN (2010) The kinetics of lubricant penetration action during machining. Lubr Sci 9:127–140
42. Chen YP, Zhang CB, Shi MS, Wu JF, Petersonb GP (2009) Study on flow and heat transfer characteristics of heat pipe with axial "Ω"-shaped microgrooves. Int J Heat Mass Transf 52:636–643

Publisher's note Springer Nature remains neutral with regard to jurisdictional claims in published maps and institutional affiliations.